Making sense of the spectra of Betelgeuse and other Red SuperGiants[⋆]

A. López Ariste[1], Q. Pilate[1], A. Lavail[1], Ph. Mathias[1],

IRAP, Université de Toulouse, CNRS, CNES, UPS. 14, Av. E. Belin. 31400 Toulouse, France

ABSTRACT

Context.
Aims. Spectropolarimetry of atomic lines in the spectra of Betelgeuse and other Red SuperGiants presents broad line profiles in linear polarization, but narrow profiles in intensity. Recent observations of the Red SuperGiant RW Cep show on the other hand broad intensity profiles comparable to those in linear polarization. This observation hints that the previous inconsistency observed in other Red SuperGiants is just a temporary situation of the atmosphere of a given star. We propose an explanation for both cases based on the presence of strong gradients, larger than the thermal broadening of the spectral line. Using analytical but
Methods.
Results.
Conclusions.

1. The issue with the spectra of Red SuperGiants.

The discovery of linear polarisation in the atomic lines of the spectrum of Betelgeuse (Aurière et al. 2016) opened the path to a succesful imaging technique that has provided continuous images of the convective structures in the photosphere of Betelgeuse (since 2013) and other Red SuperGiants (RSG) (López Ariste et al. 2018). More recently, exploiting the different formation heights of different atomic lines, 3-dimensional images of the photosphere have been inferred from those spectropolarimetric signals (López Ariste et al. 2022). Beyond the images themselves, this technique has unveiled the large convective velocities predicted by numerical simulation codes and confirmed the size and temporal scales of variation of these convective structures. The measurement of plasma velocities at different heights has also uncovered plasma plumes that barely change velocity as they rise through the atmosphere of Betelgeuse, pointing to the presence of an acceleration mechanism hitherto unidentified but present from the photospheric heights and able to equilibrate forces with gravity and maintain plasma velocities as they approach the height at which they will definitely escape as stellar wind.

These successes were founded in a series of approximations about the polarized line formation which have been discussed and partially justified the cited literature REFERENCE. Among them, perhaps the weakest is the imposition of a relationship between brightness and vertical velocity. Such correlation is observed whenever the line formation happens while convection is still the dominant dynamical process, as in the Sun. Numerical simulations of the photosphere [REFERENCE] of Betelgeuse appear to infirm such relationship and suggest that the line formation region of most of the atomic lines present in the spectum resides above the convective zones, and brightness and velocity would not be clearly correlated in the formation of spectral lines in Betelgeuse. Against this prediction stands the comparison of images inferred from spectropolarimetry assuming this correlation true, and the reconstructed images obtained through interferometry.

Kravchenko et al. (2018) explored whether convection still leaves a signature in the intensity spectra and, through a newly-developed tomographic technique, unveiled a histeresis loop reminiscent of what could be expected if lines were formed in convective conditions, when the correlation of brightness and vertical velocities is still valid. Such histeresis loops could be seen in observed spectra and also, marginally, in synthetic spectra computed by radiative transfer through stellar snapshots numerically simulated. But these same authors claimed that such histeresis loops may be understood not as reflecting that lines form where convection takes place, but rather that acoustic waves or pulsations may propagate correlations of the kind to selected patches well above where convection dominates and where atomic lines form. Since, traditionally, convection has also been called for to explain the C-shape line asymmetries [REFERENCE GRAY?], it should go without further justification that it is in the intensity profile that we should seek the answer to the validity of the brightness-velocity correlation at the core of the interpretation of the measured linear polarization in terms of images of convective structures.

However, inspection of the observed intensity and linear polarization profiles makes it clear that there is a further problem with intensity profiles than just correctly interpreting bisectors or histeresis loops. As emphasized by **?**, the intensity profiles observed on Betelgeuse are astonishingly narrower than the width of the linear polarization signal. This is illustrated once again in Fig. 1, where the limits of v_0, the assumed velocity of the star, and v_{max}, the assumed highest velocity of the rising plasma are also shown. These two limits are set by simple inspection of the accumulated data set of linear polarization profiles. In a model of pure convective movements, all that is bright is rising vertically, and the most blushifted signal observed must come from plasma rising at exactly disk center at the maximum velocity possible. Thus, no linear polarization is to be observed at shorter wave-

---

[⋆] Based on observations obtained at the Télescope Bernard Lyot (TBL) at Observatoire du Pic du Midi, CNRS/INSU and Université de Toulouse, France.

lengths than this v_{max} limit. Similarly, plasma at the limb of the star emits at zero velocity respect to the bulk star's velocity v_0. This red limit is not strict: sinking plasma, though darker than rising plasma, produces signals redder than this limit. And **?** interpreted the spectra of the RSG μ Cep as the intermittent plumes arising in the back hemisphere of the star, but rising high enough to be visible above the limb. López Ariste et al. (2022) discussed at length the validity and justification of the assumed limits for Betelgeuse. In what concerns here, nevertheless, it is most obvious that whatever the precise value of v_{max} , there is a considerable amount of linear polarization arising at wavelengths which, judging from the intensity profile alone, are in the continuum, beyond the blue wing of the line. This is just nonsense. Continuum is precisely defined by its quasi-independence of wavelength, at least at the scales here concerned. The observed linear polarization signal varies rapidly with wavelength and cannot be due to any continuum emitting process. Interpreting it as the polarisation of the extreme wing of the spectral line makes no much sense either. It would require polarisation levels of 10% at some wavelengths, which is also nonsense. There is no mechanism by which such high levels of linear polarization can be created in the extreme wing of the line, when elsewhere in the line the observed polarisation amplitudes are 0.1% at most.

This is the problem we address in the present work. We propose a mechanism by which the intensity profile, after integration over the disk, is narrowed while the linear polarisation profile keeps the original width. Such mechanism is based upon two ingredients. The first one is that the integration over the disk favours signals emerging from the disk center, since the wavelength of emission is modulated by its projection onto the line of sight, and the $\cos\theta$ function reaches a maximum at disk center. Hence velocities around disk center, if relatively homogeneous, are similar and add up together, while at the limb a small change in position considerably changes the projected velocity, even if the atmosphere is homogeneous. This effect is common to all disk integrations, so, alone, it makes no difference between Betelgeuse and any other star. The second ingredient is critical: it requires the presence of gradients of velocity in the region of formation of the line larger than the width of the local line. These gradients deformate the line profiles giving them a triangular shape. Due to it, and in a nutshell: regions at disk center with large gradients produce triangular shape profiles that contribute to all wavelengths, while regions at the limb with low gradients produce narrow gaussian profiles centered at near zero velocities. The correct addition of these contributions produces the observed profiles as we shall demonstrate in the next section.

In the process to understand the intensity profiles of Betelgeuse, a key element has been the observation of another RSG, RW Cep. This star is not particularly different than Betelgeuse or any other well classified RSG. Any differences between Betelgeuse and RW Cep, as with any other star must be mostly attributed to whatever the star is doing right now: is it quietly convecting as Betelgeuse appears to do (except perhaps during the recent great dimming event), or is it in a Decin stage as μ Cep, with repeated events of large plumes raising sufficiently high to escape gravity and form a new shell of dust clumps. It was a big surprise to discover therefore that RW Cep presents in our 2023 observations a large and broad profile, fully compatible with the linear polarisation signals and unlike anything observed in Betelgeuse in the last 10 years. RW Cep is doing something right now which broadens the profiles. Atmospheric dynamics, in its most broad sense, are therefore able to broaden or narrow intensity profiles. The narrow profiles are not intrinsic to an RSG, they are rather due to the present dynamics of the star. This realisa-

tion opened the path to our proposed solution. In Section 3 we explore how our proposition based upon velocity gradients can explain both Betelgeuse and RW Cep intensity profiles.

Two last observational facts are discussed and modelled in Section 4. Bisectors of Betelgeuse line profiles often present a typical C-shape, but from time to time they reverse their asymmetry. When looking into lines formed in particular regions, the situation appears clearer in that deep lines (meaning lines forming deep in the photosphere) present systematically a C-shape bisector, while high lines present a reverse-C bisector. When adding them together, it will depend on the differential brightness of high to deep lines that the compound spectral line presents one or the other asymmetry. Our proposed solution must explain these differences and their change in time. And finally, the intensity line presents a velocity span of 7-10 km s^{-1} over time. Since linear polarisation signals confirm the 40 km s^{-1} velocities predicted by numerical simulations to be present in the convective atmosphere, this velocity span cannot be a direct projection of the dynamics of the atmosphere but rather the result of some kind of averaging that our solution must explain as well.

2. Radiative transfer in the photosphere of an RSG.

Our approach to the problem of radiative transfer in these atmospheres responds to a constraint and a desire. The constraint is that, in spite of all its successes and of the harbinger of ever greater and precise details, we cannot consider numerical simulations as the ultimate description of red supergiants. Not just that sufficient simulations with the appropriate parameters are not yet available but also that it is our purpose to always check those models and not to assume them true and limit observations to a perennial validation of the models. The desire is for an explanation rather than a description or a perfect fit. We do not desire at this point to reproduce the intensity profiles quantitatively, but to identify the key physical ingredients responsible of the main observed features.

With those criteria in mind, we can boldly split the problem of radiative transfer in two classes of problems. One is the variation of the opacity with time and position along and across the photosphere of our RSG; the second is the integration of the local line profiles along each line of sight and the addition of all the lines of sight over the stellar disk, what we can dub the geometry part of the radiative transfer problem. If we make the choice of doing full radiative transfer on a numerical simulation, both aspects of the problem, the geometry and the opacity, are inevitably together and we loose perspective on their relative importance. As it comes, we shall see that the geometry is mostly responsible of the main features observed in the atomic line profiles of Betelgeuse, playing opacity variations a second role.

We therefore reduce the transfer problem to its bare bones. We assume that the opacity is constant along the line of sight and all over the stellar disk, in spite of the obvious presence of density and temperature variations. We assume a normalized continuum emitted below the region of formation of the line. We parameterize this region of formation with a geometrical distance z which will vary from 0 through 1, $z = 0$ being at the strict bottom end of the region of formation, and $z = 1$ being at the strict top end. At each line of sight, the emergent spectrum will look like

$$I(v) = e^{-\tau(v)} \tag{1}$$

where $\tau(v)$ is the total opacity along the line of sight, and we chose to parameterize wavelength in terms of velocity differences v respect to the local reference frame (where $v =$

Fig. 1. Observed profiles

0 km s^{-1}).The total opacity is computed as

$$\tau(\nu) = \int_{z=0}^{z=1} k\phi[\nu - v(z,\theta,\chi)\cos\theta]dz \qquad (2)$$

where k is the constant absorption coefficient, and $v(z,\theta,\chi)$ is the radial velocity of the atoms at height z, angular distance to the disk center θ and position angle χ. Finally we approximate the line profile ϕ by a simple gaussian of standard deviation $\Delta = 6$ km s^{-1}(López Ariste et al. 2018)

$$\phi(\nu) = e^{-\frac{\nu^2}{\Delta^2}}. \qquad (3)$$

All those local intensity profiles, integrated over z, for each position over the disk (θ,χ) will be added together to form the disk-integrated line profile that we will compare to the observations.

Our approach is guided by the work of Bertout & Magnan (1987) (see also Wagenblast et al. (1983) and Chandrasekhar (1945)) to interpret the doubling profiles periodically observed in Mira stars. Those authors also strip radiative transfer to its bare fundamentals to demonstrate the somehow unexpected result of combining disk integration and velocity gradients along the line of sight. In their work they address Mira stars, whose atmosphere is supposed to be made of an expanding (or contracting) shell of gas on top of the star. This shell is assumed to be homogeneous in velocity and geometry, what allows the integral over the disk to be intimately intricated with the integral along the line of sight. This helps in their solution to the problem. In our present case we shall also call for strong gradients of velocity along the line of sight, but these will only appear in coincidence with the plumes of hot, rising plasma, and will not be homogeneous nor in their distribution over the disk nor in their velocities. For this reason we shall decouple the integration over the line of sight from the integration over the disk. And in this aspect we diverge from the work of Bertout & Magnan (1987). Despite that difference, we shall recover most of the features described by those authors.

It is worth to solve analytically the integral in Eq. (2) for several gradients of the velocity with z. In the first and straightforward case the velocity is constant with z, but projects itself onto the line of sight. We find that

$$\tau(\nu) = k(z_1 - z_0)\phi[\nu - v(z,\theta,\chi)\cos\theta] \qquad (4)$$

As one adds profiles for different values of θ one recovers a flat-bottom or square profile. This is what one would expect from a constant and homogeneous rising velocity of the plasma. This is not what one sees, but yet one does not expect the velocity to be constant with z.

Hence, our second case assumes a linear dependence of the velocity with z in the form $v(z) = v_0(1 - z)$ which ensures that the velocity dimishes with height. The integral comes out to be

$$\tau(\nu) = \frac{\Delta k}{v_0 \cos\theta} \frac{\sqrt{\pi}}{2} \left[erf\left(\frac{\nu}{\Delta}\right) - erf\left(\frac{\nu - v_0\cos\theta}{\Delta}\right) \right] \qquad (5)$$

where erf stands for the error function. Whenever v_0 is smaller than Δ this is just a slightly deformed gaussian that keeps adding up for all and every point over the disk. However if v_0 is larger than Δ we find that for large values of θ, near the limb, quasi-gaussian profiles are produced, but near disk center, when $\cos\theta \approx 1$, bottom flat profiles are produced. Adding up over all

values of θ results in a disk-integrated assymetric profile that can be seen in Fig.2

However a linear dependence of the velocity with z is not what one naively expects from plasma balistically sent upwards during convection. One rather expects a square root dependence, $v(z) = v_0\sqrt{1 - \beta z}$, where β modulates the final velocity of the plasma. Such velocity can also be readily integrated and the total opacity per line of sight comes out to be

$$\begin{aligned}
\tau(\nu) &= \frac{\Delta k\nu\sqrt{\pi}}{\beta v_0^2 \cos^2\theta} \left[\mathrm{erf}\left(\frac{\nu - v_0\cos\theta\sqrt{1-\beta z}}{\Delta}\right) \right.\\
&\left. -\mathrm{erf}\left(\frac{\nu - v_0\cos\theta}{\Delta}\right) \right] + \\
&+ \frac{\Delta^2}{\beta v_0^2 \cos^2\theta} \left(e^{-\frac{(\nu - v_0\cos\theta\sqrt{(1-\beta z)})^2}{\Delta^2}} - e^{-\frac{(\nu - v_0\cos\theta)^2}{\Delta^2}} \right) \quad (6)
\end{aligned}$$

One readily notices the linear dependence on ν on the first term of this solution, a fact already brought up by Bertout & Magnan (1987) in their geometry and which is maintained despite the divergences between our two approaches. The resulting profiles, if this term dominates over the second, show a characteristic saw-tooth shape that can also be seen in Fig.2

When changing the gradients of the velocity along the line of sight, even with no modification of the maximum velocities involved, which is always 40 km s^{-1}in the examples of Fig.2, we witness dramatic changes in the shape of the profiles. Although always asymmetric, the examples in Fig. 2 show the path towards narrowing the disk-integrated line profile. Furthermore, and in advance of the results in Sect. 4, we see how the bisector can be modified without changing neither the velocities or the absorption coefficient. A ballistic drop in velocity near disk center produces a C-shape bisector if it dominates the integrated brightness so that any limb contribution is small. But a linear drop in velocity near disk center will produce an inverse C-shape integrated line if the limb contributes with similar brightness to the disk integrated profile. The combination of strong gradients of different dependence with z, brightness inhomogeneities and disk integration appears to be what is needed to reproduce the observed intensity profiles in different RSG.

3. Reproducing the observed intensity profiles.

Figures 1 and 3 shows selected examples of profiles of Betelgeuse and RW Cep respectively, which represent the two extremes of profile shapes observed in RSGs with Narval and its updated version, NeoNarval (see López Ariste et al. 2022; **?**, for a description of both instruments and the data reduction procedures). What we are presenting in all our plots are cross-correlation profiles made by the addition of many different spectral lines (Josselin & Plez 2007)[RFERENCE DONATI??]. Most often all those lines are added up irrespective of their line depression, formation height or any other attribute. This is what has been done in the case of the profiles shown in Fig. 3. In the case of Betelgeuse, the presented profiles date from 2013 and 2014. This data has been presented before by Aurière et al. (2016) who discuss also the line lists used in the cross-correlation. Though Betelgeuse is being observed periodically in recent years, after the great dimming event of the end of 2019 the levels of linear polarisation have drastically diminished. Since it is our purpose
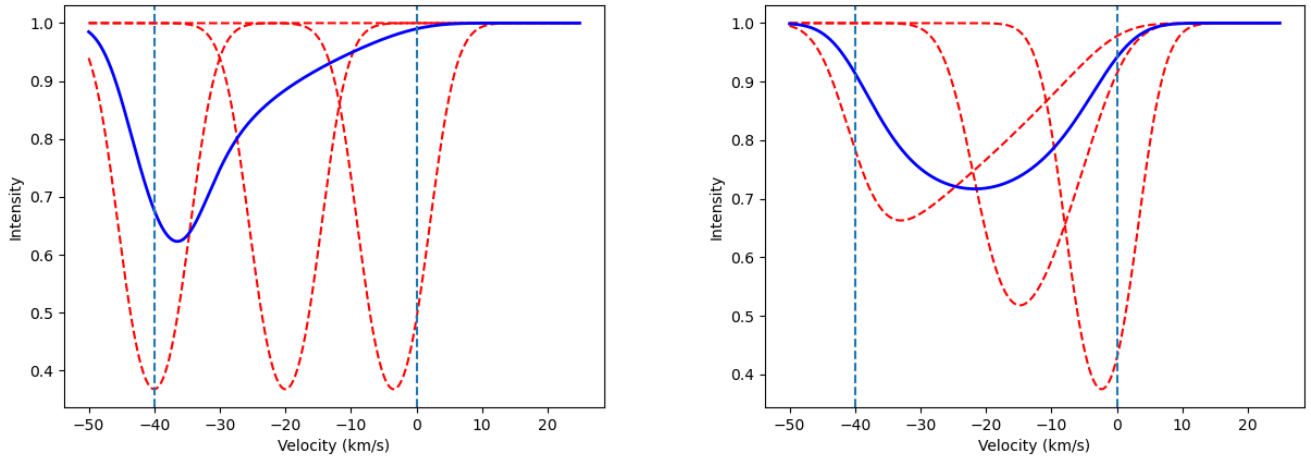
Fig. 2. Examples of asymmetric profiles generated when strong gradients are present along the line of sight. On the left a linear gradient (or rather a constant velocity?) from the maximum velocity to zero in the region of formation is used. On the right the gradient follows a square-root law. Dashed red lines are used for individual lines of sight from disk at disk center, $\theta = 45°$ and close to the limb. Continuous, blue lines show the disk-integrated profile. The vertical dashed lines mark the radial outward velocity of the plasma $v_{max} = -40$ km s^{-1} in the observer framework, and the zero velocity v_0.
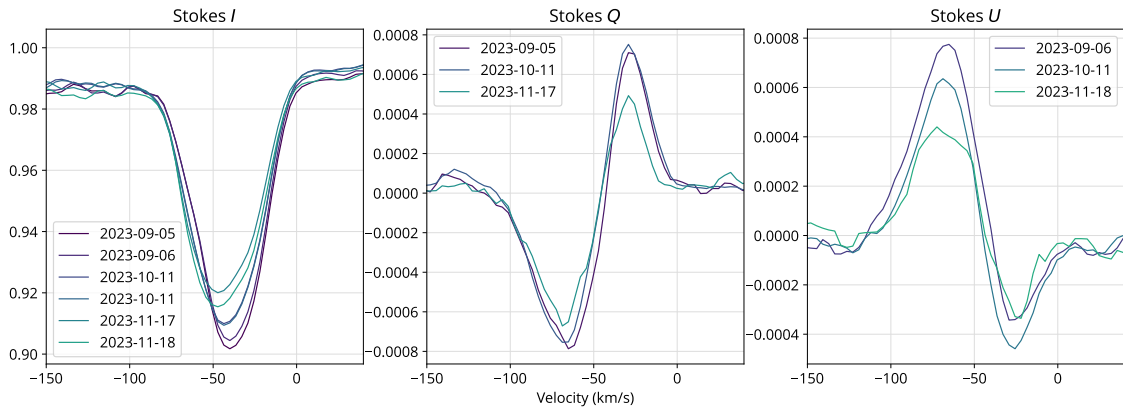
Fig. 3. Examples of profiles of RW Cep observed with NeoNarval in 2023. Intensity is on the left plot, Stokes Q and U are shown in the center and right plots.

to illustrate the difference in wavelength span between the linear polarisation and the intensity profile, we have preferred the old data to better illustrate this discrepancy. Intensity profiles of Betelgeuse keep being in 2023 as narrow as in 2013. For our second star, RW Cep, we present NeoNarval data from 2023, August 18th through November, 18th.

We have seen that the presence of velocity gradients larger than the width of the line and of different dependences with z opens the door to a variety of profile shapes, from purely gaussian to saw-tooth shapes, from broad to narrow ones. Which one is present in the observation of an RSG at a given date depends on the distribution of both gradients and brightness over the disk at the moment of the observation. For the sake of simplicity we are going to fix gradients to be of the ballistic kind, with a square root dependence on z. But we are going to vary both the amplitude of the gradients (changing the parameter β) and the distribution of brightness and velocity amplitudes over the disk. We will select the images inferred from linear polarisation of Betelgeuse to represent what we believe are acceptable distributions of brightness and velocities over the disk, recalling that both magnitudes, brightness and velocity, are relied in the inver-

sion algorithms fitting linear polarisation as if the light-emitting plasma was in the presence of convection.

As a first illustration, using the image of the photosphere of Betelgeuse that best fits the observed linear polarisation signals observed on 27 November 2013 (Aurière et al. 2016) we present in Fig. 4 the local profiles along a radius of the visible hemisphere together with the integrated profile along that radius. In that date, and along the chosen radius, there is no much contribution at the maximum velocities. There are however several points where the plasma is sinking and which can be seen redshifted respect to the v_0 velocity. All plots are normalized, so we cannot see that these redshifted contributions have very low intensity and contribute nothing to the integrated profile.

As described before, the profiles close to disk center contribute to the largest, blue shifted, velocities. But due to the velocity gradients they also contribute at lower velocities. Profiles close to the limb contribute only to the lower velocity, near the v_0 rest velocity of the star. Altogether wavelengths near the rest velocity v_0 get a larger contribution in the integration, and the net result is a narrow profile blue-shifted but with the rest velocity v_0 in its red wing.
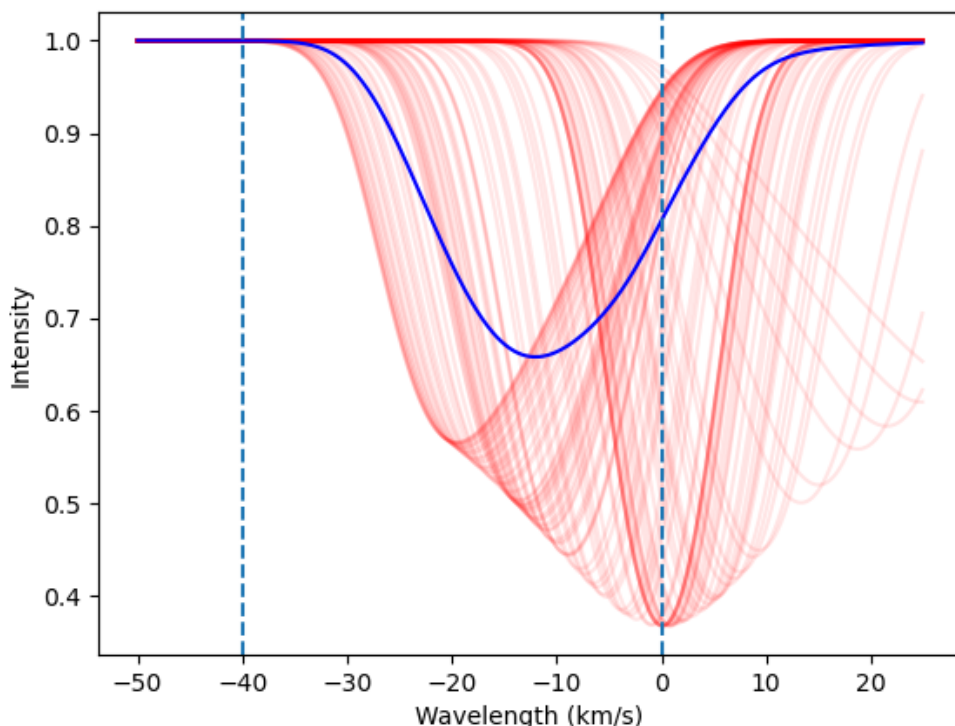
Fig. 4. Example of local (red) and integrated (blue) profiles along the vertical radius of the image of Betelgeuse that fitted best the observations of linear polarisation on 20th December 2013. All profiles are normalized to the continuum value for the sake of the visibility of the plot.

We can now, extend the calculation to the whole disk and explore the impact of the velocity gradients, Fig. 5 shows the case of $\beta = 1$, that is the velocity at each point drops from the value found in the inferred image to zero in the span of the formation region of the line. This is quite a large gradient near disk center, with maximum velocities reaching $40\,\mathrm{km\,s^{-1}}$ but the gradients reduces to zero towards the limb. The disk-integrated profile will be a combination of saw-tooth and gaussian profiles as in Fig.2. But the distribution of brighness is not homogeneous, and some profiles will be given more weight than others. The result can be seen in Fig. 5 where 10 observations, from 27 November 2013 through 3 March 2015, presented by Aurière et al. (2016) are used as examples of brightness and velocity spatial distributions.

We have chosen the opacity value k in Eq. (2) so that the disk-integrated profile matches the depth of the observed intensity profile. Otherwise all parameters are those used by the inversion code to fit the linear polarisation profiles: maximum velocity amplitude and width of the Gaussian profile. The comparison of these so-computed profiles and the observed ones is remarkable. The computed profiles are narrow, in spite of the span of velocities used for the computation. This is due, as we keep repeating, to the combination of large velocity gradients and the brightness distribution over the disk. The zero velocity falls in the red wing of the line rather than on line-center. This justifies *a posteriori* the ad-hoc choice made in the inversion codes by López Ariste et al. (2018). Here, this is an emergent feature, there is nothing in the computation that forces the position of the minimum of the disk-integrated profile. The same can be said about the maximum velocity, that falls over the continuum well beyond the blue wing of the line, in spite of the presence of large velocities at some points over the disk. We conclude from this comparison,

that our basic model captures the main features of the observed profiles of Betelgeuse. This is in spite of imposing a constant absorption coefficient over the atmosphere, and of imposing the same velocity gradient dependence for all points. We shall look later into the bisector shape and the velocity spans to further push this comparison. At this point we can however dare to extract a far-edged conclusion. The model for linear polarisation is based upon the assumption that this linear polarization emerges from Rayleigh scattering of the continuum. The continuum polarised photons are subsequently absorbed by atoms higher in the atmosphere which re-emit them unpolarised. The local continuum polarisation is in this manner deleted in the spectral line, and it is this de-polarisation signal that we measure with our instruments. While the polarization amplitude, in that model, is mostly attached to the brightness of the continuum emitting plasma, the Doppler shift of the de-polarized photon is that of the absorbing and re-emitting atom. Linear polarisation profiles present a broad span of velocities, but the present comparison of computed and observed intensity profiles appears to require a gradient of velocities down to zero over the region of formation of the line. We must conclude in consequence that de-polarised photons are coming from the very first lengths of this formation region, while the photons making the spectral line come from the integration along the whole region.

RW Cep presents the other end of the variation seen in the intensity profiles of RSGs. We see, in the recent observations of this star, broadened profiles with a span comparable to the one observed in the linear polarisation profiles (Fig. 2). Josselin & Plez (2007) also presented intensity profiles for RW Cep, though without linear polarisation, that can be compared to the ones presented here to appreciate all the variability of which this RSG
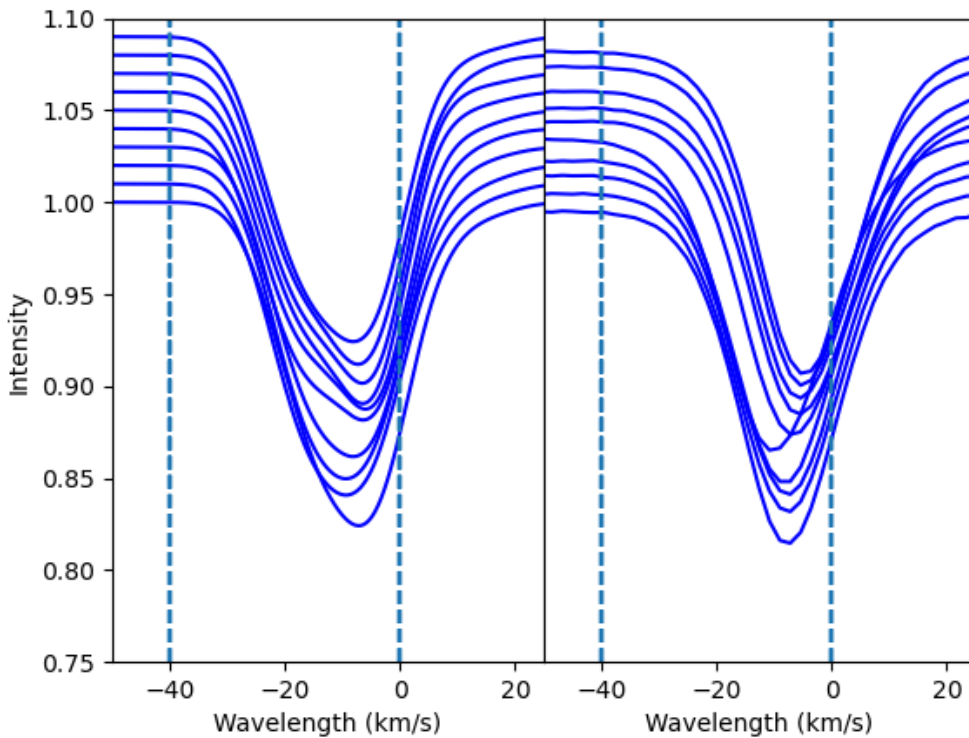
Fig. 5. Left: Inferred images of Betelgeuse from 27 November 2013 through 3 March 2015 are used to integrate profiles assuming that at every point the gradient is such that the velocity reduces to 0 at the top of the formation region of the line ($\beta = 1$). Profiles are shifted in ordinates for clarity. Right: The actual observed intensity profiles in those same dates.

is capable, unlike the stable profiles of Betelgeuse. In Fig. 6 we repeat the calculations of disk-integrated profiles with the same brightness and velocity distributions used for Betelgeuse in Fig. 5 (and therefore inferred from the fit of the observed linear polarisation of Betelgeuse), just changing the value of from $\beta = 1$ to $\beta = 0.2$. This value of β means that rather than dropping to zero along the formation region of the spectral line, the velocity diminishes of just 10%. With such small gradients we recover the flat-bottom profiles that we can favourably compare to the observed profiles of RW Cep. Whenever the brightness distribution is such that hot large spots are present over the disk, one can even find split profiles. These are not seen in the present observations of RW Cep, but we notice that Kravchenko et al. (2018) presents observations of another RSG, V Tau, with some split line profiles that could be compared to the ones we compute here.

This second favourable comparison between our simple model and observations gives further support to it. In our view it confirms the hypothesis that the geometry of the radiative transfer and, in particular, the combination of the brightness distribution and the actual gradients of velocity present at the particular moment of the observation, are sufficient to qualitatively reproduce the observed intensity profiles.

The scenario for the polarized line formation that emerges from these tests is the following. A continuum forms deep in the atmosphere of Betelgeuse [Or more generally in RGs?]. This continuum is polarized by Rayleigh scattering and it is at this point that the information on brightness inhomogeneities is dump into the polarization amplitude. This does not have to be the continuum that finally emerges from the star. It is a contin-

uum that may form deeper since it is depolarized by the line-forming atoms at the deepest point of its formation region. This is so because linear polarization signals do not suffer from integration along the line of sight and conserve the signature of the largest velocities found at the deepest point of the line formation region. This is coherent with the hypothesis of a single scattering event in the creation of the polarization signal. It is at this point that the wavelength position of the polarization signal is acquired and, from it, the position over the stellar disk to which this polarization will be assigned. Both the brightness of the image inferred from linear polarization and its position over the disk would come, in this scenario, from deep photospheric layers: the brightness from a deep continuum, well beyond the typical values of opacity of the emergent continuu, and the position over the disk from the very first scattering on a line-forming atom at the bottom of the formation region. From this point on, there is no further change in the linear polarization profile, but the intensity profile keeps changing as it moves along the line formation region taking its definitive triangular or gaussian shape at the top of the formation layer, when plasma velocities have been greatly reduced.

4. Bisectors and velocity span

Observed bisectors bring up harder constraints into the line formation process. Figures 7 and 8 show the measured bisectors on intensite profiles of Betelgeuse in the period XXXX. In Fig. 7 the cross-correlated intensity profiles are made with a line mask that selects lines formed in the upper part of the atmosphere. This mask was selected and created by Kravchenko et al. (2018).
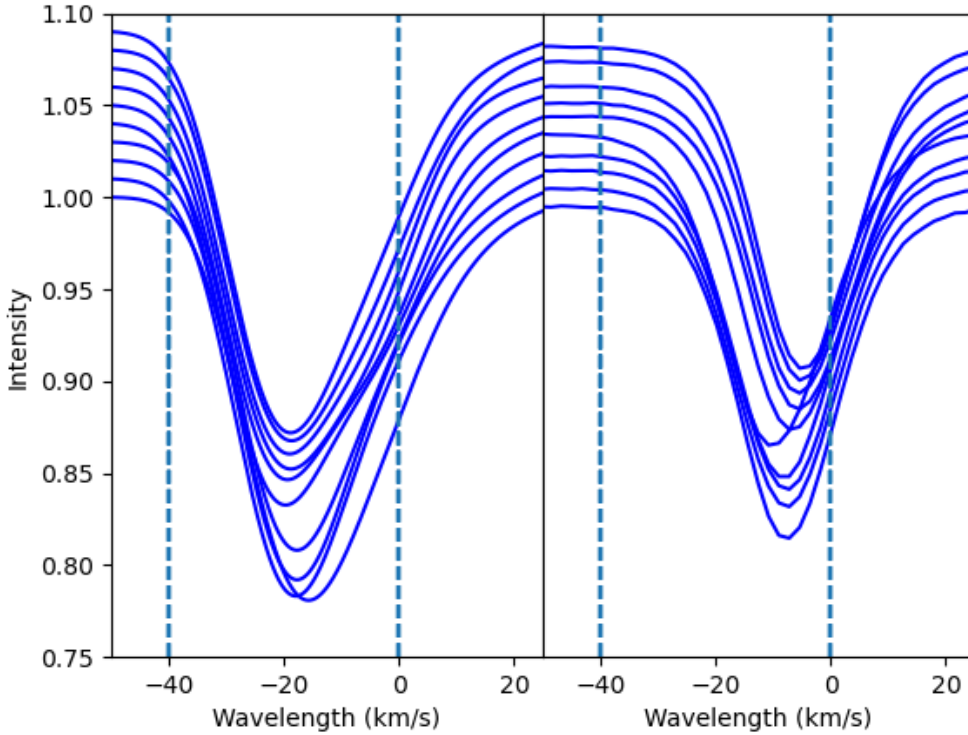
Fig. 6. Left: Same as Fig. 5 but for $\beta = 0.2$. Right: THESE ARE NOT THE OBSERVED PROFILES OF RW Cep but just the profiles of Betelgeuse

Strongly curved inverse C-shape bisectors are seen in the lines formed in this top photospheric layer, a feature traditionally interpreted as the presence of accelerating rising plasma. In Fig. **??** lines forming deeper in the photosphere have been selected, by the simpler procedure of selecting lines with central depressions in the range of 0.6 to 0.7 the continuum intensity. In these deepest layers, and for all the periods observed, the bisectors are straight with a tendency to bend towards the red in the top parts in what looks as the more common C-shape bisectors.

Reproducing not just the width of the profile, as done in the previous section, but also the bisector asymmetry is harder with such a simple radiative transfer model as the one we have chosen. Above, the presence of strong gradients was seen as a requirement to make compatible the broad linear polarisation profiles and the narrow intensity profiles of Betelgeuse, while reducing those gradients was the simple change required to also explain RW Cep profiles. This main conclusion also applies when trying to reproduce bisectors. Fig. 9 shows the bisectors of disk-integrated profiles using the inferred image of Betelgeuse for the date of XXXX. While the square root gradient law is used in all the cases, the value of β is changed to simulate several situations, from almost no gradient ($\beta = 0.1$) to a full decrease to zero velocity along the line formation region ($\beta = 1$). Affording very low gradients while maintaining the gaussian shape of Betelgeuse profiles and not drifting towards RW Cep-like profiles requires reducing the maximum velocities to 70% the original values. With this difference taken into account, the computed bisectors can be favourably compared to the observed ones of Fig.8, particularly for values of $\beta \sim 0.5$. Such lower values of β may be justified by the smaller region covered by the formation region of these lines. But one must not over-interpret the comparison of real data with such a simple radiative transfer problem.

The important conclusion is that observed bisectors are still sufficiently well reproduced by the simple model requiring strong gradients and the actual plasma velocities and brightness inhomogeneities inferred from the fit of the linear polarisation profiles.

The top photospheric layers present a pronouncedly inverse C-shape at all dates. These lines sometimes dominate the total line made of the addition of all available lines in the spectrum, which explains that the bisector of this cross-correlated line may present at particular dates an inverse C-shape, though often it presents a normal C-shape. But when isolated in separate layers, the bisectors maintain their shape at all dates. This inverse C-shape is traditionally interpreted as the presence of accelerating and rising plasma. And so appears to be the case in our simple model as well. To reproduce these inverse-C bisectors we need to abandon the square root decrease in velocity and use a gradient that increases the velocity linearly as $v(z) = v_0 \beta z$. The resulting bisectors can be seen in Fig. 10. For constant velocities ($\beta = 0.1$) the bisector is almos straight. As the gradient increeases and, particularly, for $\beta > 1$ inverse C-shape bisectors appear. These do not reproduce completely the observed bisectors of Fig.7. One is tempted to suggest that the lines in the upper photosphere start forming while negative gradients are still present, but that mid way along their formation region the gradient changes sign and actual plasma acceleration appear.

The last observed phenomenon we address is the time variation of the line core velocity and the hysteresis loop discovered by Kravchenko et al. (2019) when plotting temperature vs. line core velocity. This last hysteresis loop is one of the most clear signatures to date of convection dynamics in the intensity profiles. It prompted the authors to question how it was possible to observe it given that the line formation regions were
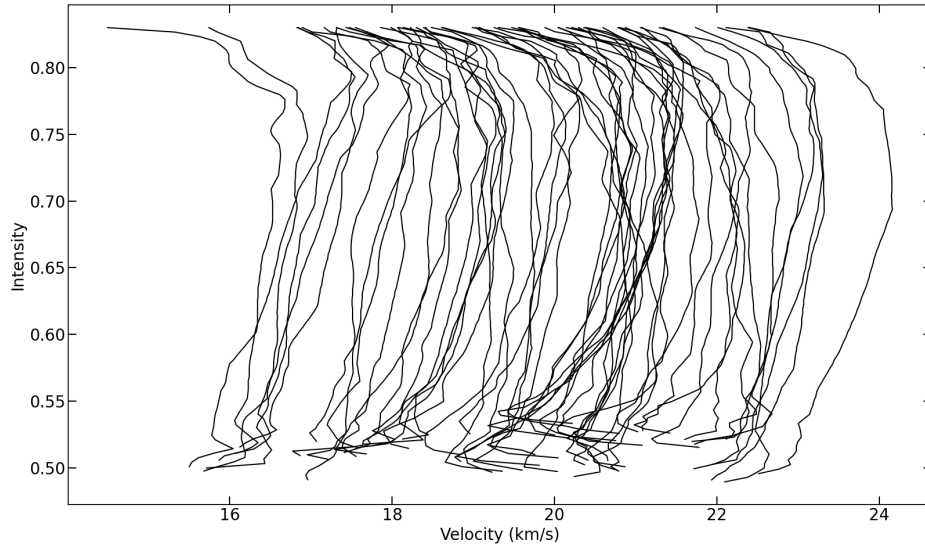
Fig. 7. Measured bisectors in the cross-correlated intensity line profile of spectra of Betelgeuse from the period XXXXXX. The cross-correlation uses Mask XXXXXX from Kravchenko et al. (2018) that selectes lines forming high in the photosphere of the star. [COUCHES 0.7-1.0?]
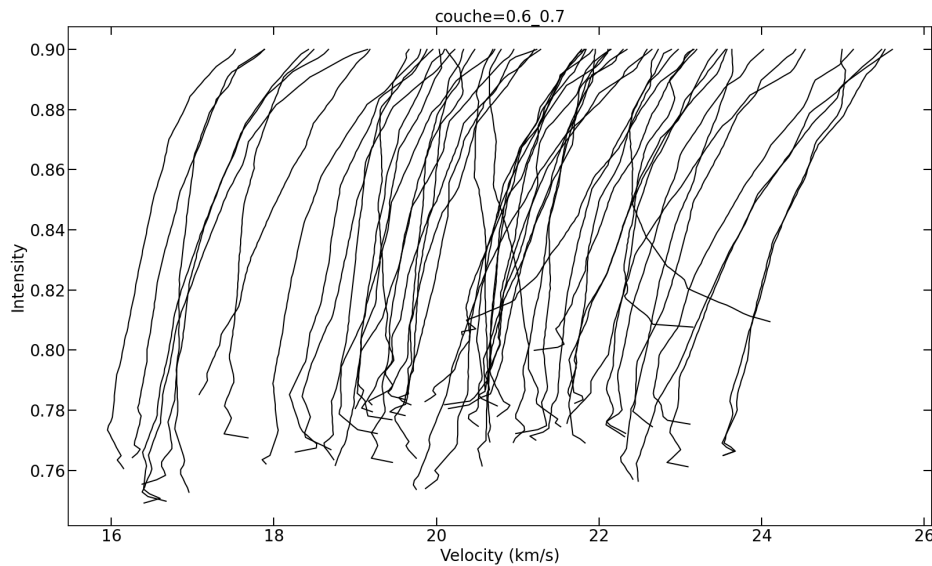

Fig. 8. As in Fig. 7, but the mask used for cross-correlation selects atomic lines with central depressions in the range 0.6 through 0.7 of the continuum. This filter approximately selects lines forming deep in the photosphere of the star.

above the regions which, as per numerical simulations, are dominated by convective dynamics. The answer given by Kravchenko et al. (2019) was that at the heights of formation of the investigated lines velocities and brightness could still be proxies of the convective dynamics brought up from deeper layer by acoustic waves.

In our present radiative transfer modelling, the integrated intensity line does not represent actual plasma velocities, but a more complex parameter involving mostly velocity gradients and the brightness distributions over the disk. In the case of narrowed profiles, as those of Betelgeuse, we shall not expect, and we do not observe , the line core to move across the whole span

of plasma velocities, but just across a small residual span. Using the same series of images of Betelgeuse inferred from linear polarisation that we have used throughout this work (Aurière et al. 2016) we, once again, integrate over the disk with strong parabolic gradients ($v(z) = v_0 \beta z^2$ with $\beta = 1$). In Fig. 11 we present the line core velocities measured over these profiles and also plot those values against the value of the continuum (in Fig. 5 this continuum was normalised, we now keep it).

The span of velocities obtaine from these numerical test is smaller than the observed one (3 to 5 kms vs. 7 km s^{-1}) which certainly points to the insufficient sophistication of our radiative transfer and of the brightness distributions used. A velocity
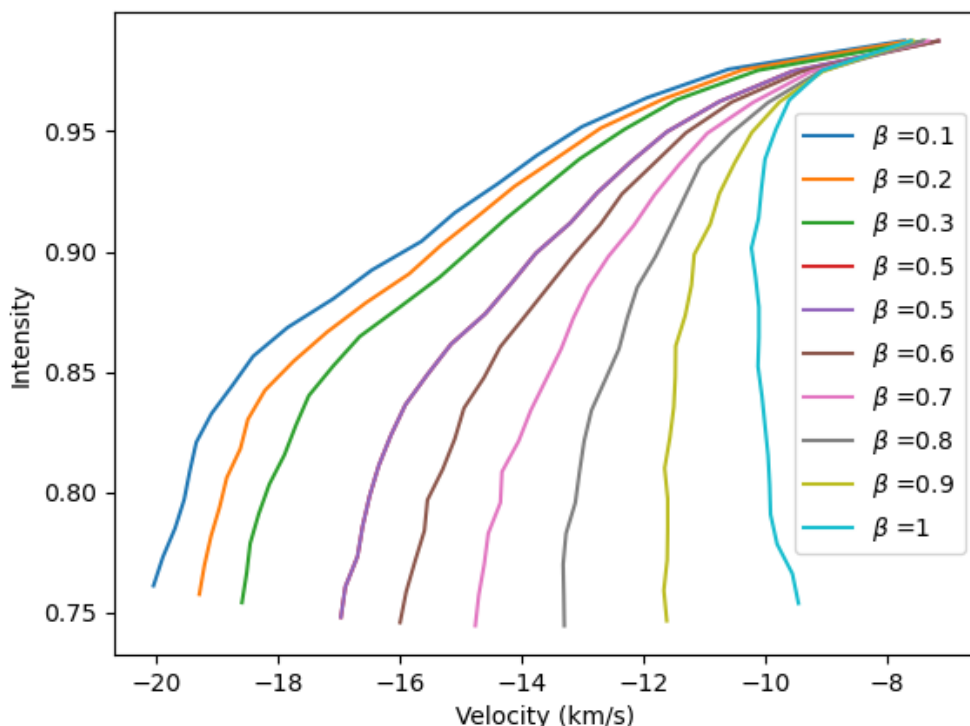
Fig. 9. Bisectors computed using the image of Betelgeuse inferred to best fit the linear polarisation signal observed on 20 December 2013. Parabolic gradients reducing the radial velocity are using with various values of β as indicated. The maximum velocities at each point over the disk have been reduced to 70% the inferred value from the fit of linear polarisation signal to avoid the broadening of the profiles in the cases with small β, thus keeping the computed profiles narrow, as the observed ones. vels*0.7

span is nevertheless present and we are satisfied that our simple model captures the phenomenon of these vagaries and provides an explanation under the same framework that has successfully explained the narrow and broad profiles, and the bisectors. Using the continuum as a rough proxy of temperature, we can also guess at the presence of the hysteresis loops discovered by Kravchenko et al. (2018). Rather than a loop, the computed profiles appear to show two clusters of profiles at similar line core velocities but different temperatures/continua. These two clusters are joined directly when increasing temperature and through a rapid excursion to large line core shifts when decreasing the temperature. This is not unlike what Kravchenko et al. (2019) presented, both from numerical simulations and observations, although in our case the term *loop* may not be the best description of the results. It is not impossible that the phenomenon is present in our simple calculations, but the comparison clearly points to the limitations of the present approach.

5. Conclusion

A bare-bones radiative transfer scheme appears to be able to describe the main observed features of intensity line profiles in Red Super Giants (RSG). The main feature addressed in this work is the at present unexplained narrowness of the observed intensity line profiles when compared to the broad profiles seen in linear polarisation. Stripping the radiative transfer problem from most of its ingredients and, particularly, of any variation of the absorption coefficients with optical path or spatially across the stellar disk, allows us to distile the main responsible for this difference

between the profiles. We find that the combination of strong velocity gradients along the line of sight together with the brightness inhomogeneities of the stellar disk suffice to broaden or narrow the line profiles at will. Strong velocity gradients make the points around disk center to contribute to the integrated line profile with triangular profiles spanning the whole range of velocities but more intense towards redder wavelengths. Points close to the limb contribute narrow gaussian profiles at those same red wavelengths. The result is a narrow near-gaussian profile. It suffices to reduce the gradients in velocity to change the triangular profiles arising close to disk center into bottom-flat square profiles that broaden the resulting profiles and can even split the intensity line. The linear polarization profile on the other hand arises from single scattering events at the bottom of the line formation region where the velocities are larger, and no radiative transfer takes places afterwards. The wavelength position of each linear polarisation signal is defined deep in the line formation region, and the signal amplitude reflects the continuum brightness seen by atoms deep in the photosphere, hence coming from even deeper atmospheric regions. This scenario appears to justify the validity of the brightness-velocity relationship imposed to the inversion algorithm that produces images of the photopshere of Betelgeuse from the linear polarisation profiles, a relationship only valid if convection still dominates plasma dynamics.

The use of this simple radiative transfer model together with the disk brightness distributions inferred from the fit of the observed linear polarization profiles in Betelgeuse produces intensity profiles which are remarkably analogous to the observed ones. The very same model and brightness distributions can pro-
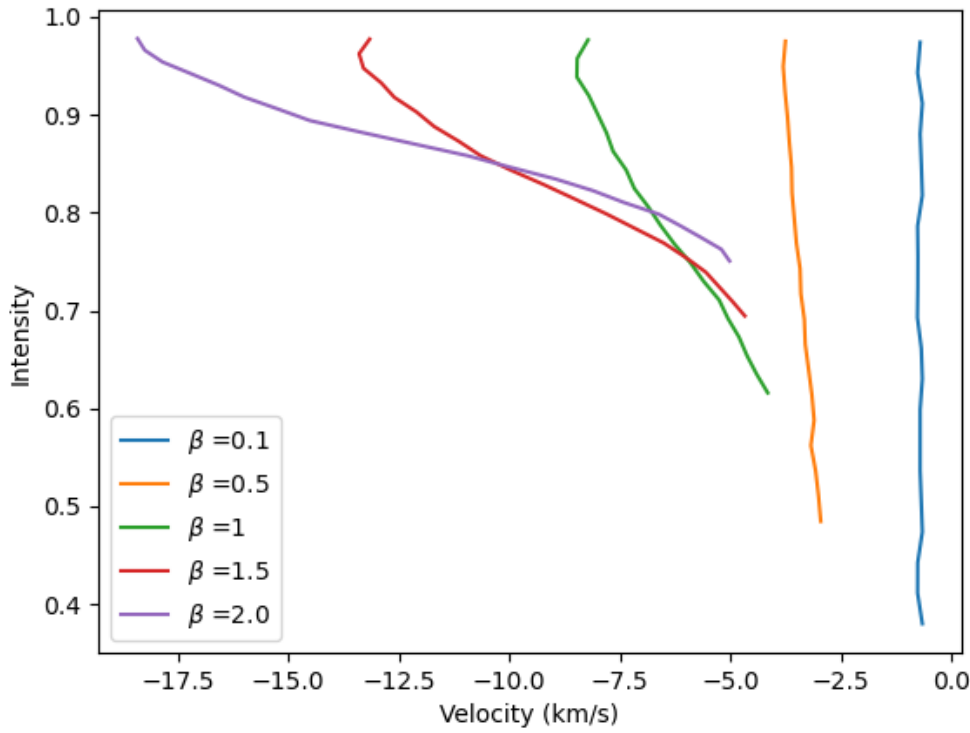
Fig. 10. Computation of bisectors as in Fig. 9 but with a linearly accelerating gradient. Several cases of spatial acceleration β are presented as indicated in the labels.
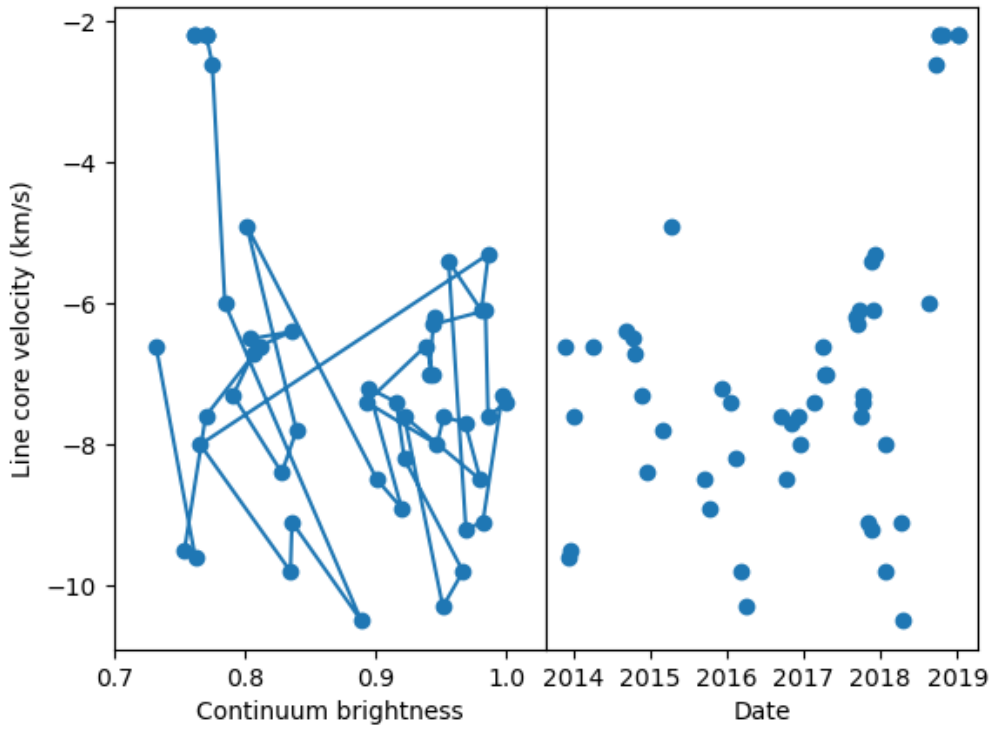

Fig. 11. Plots of line core velocities measured over the computed intensity profiles using a parabolic velocity gradient with $\beta = 1$ over the series of images of Betelgeuse presented by Aurière et al. (2016) López Ariste et al. (2023). On the left this velocity is plotted agains the continuum of the integrated profile, on the right, just in terms of date of observation.

duce intensity profiles favourably comparable to the observed ones of RW Cep by just simply altering the gradient of the velocity. These two RSG appear to represent the extremes of the variability of the intensity profiles: Betelgeuse has shown narrow profiles for the last 11 years, while RW Cep shows broad intensity profiles. Both stars show similar broad polarization profiles.

The favourable comparison of intensity profiles, computed and observed, is comforted by the measure of the lien bisectors. Again, our simple radiative transfer model succeeds by just tweaking the velocity gradients in reproducing both the C shape and inverse-C shape of the observed bisectors. The strongest inverse-C shape bisectors, observed in lines forming high in the atmosphere, appear to require a change of sign in the gradient. The decrease in velocity with height that justifies the C shape bisectors needs to be transformed into an acceleration to explain the inverse C shape. This may be (over) interpreted as these high lines being formed at regions where the stellar wind acceleration has already started. Last we have also explored how the integrated line cores shift in position over time. The phenomenon is also captured by our simple approach, but only roughly. The basic features are present, but not with the clarity of the previous comparisons. This marks the limit to which we can afford a simple radiative transfer to explain the observed line profiles.

Summing up, the observed narrow and broad intensity profiles of Betelgeuse and RW Cep in the presence of similar and broad linear polarisation profiles, does not require any change in the physics of these two red supergiants. Taking into account velocity gradients along the line of sight and integrating over an inhomogeneous disk suffices. Strong gradients explain the narrow intensity profiles of Betelgeuse, smaller gradients explain the broad profiles of RW Cep. The hypothesis of single scattering and correlation of velocity and brightness, used for the interpretation of the linear polarisation, are comforted by our results.

References

Aurière, M., López Ariste, A., Mathias, P., et al. 2016, Astronomy and Astrophysics, 591, A119

Bertout, C. & Magnan, C. 1987, Astronomy and Astrophysics, 183, 319

Chandrasekhar, S. 1945, Reviews of Modern Physics, 17, 138

Josselin, E. & Plez, B. 2007, Astronomy and Astrophysics, 469, 671

Kravchenko, K., Chiavassa, A., Van Eck, S., et al. 2019, Astronomy and Astrophysics, 632, A28, aDS Bibcode: 2019A&A...632A..28K

Kravchenko, K., Van Eck, S., Chiavassa, A., et al. 2018, Astronomy and Astrophysics, 610, A29

López Ariste, A., Georgiev, S., Mathias, P., et al. 2022, Three-dimensional imaging of convective cells in the photosphere of Betelgeuse, Tech. rep., publication Title: arXiv e-prints ADS Bibcode: 2022arXiv220212011L Type: article

López Ariste, A., Mathias, P., Tessore, B., et al. 2018, Astronomy and Astrophysics, 620, A199

López Ariste, A., Wavasseur, M., Mathias, P., et al. 2023, Astronomy and Astrophysics, 670, A62, aDS Bibcode: 2023A&A...670A..62L

Wagenblast, R., Bertout, C., & Bastian, U. 1983, Astronomy and Astrophysics, 120, 6